W. F. Hoover[1], C. B. Condit[1], P. C. Lindquist[1], A.C. Moser[2] and V.E. Guevara[3]

[1] University of Washington, Seattle, WA USA; [2]University of California, Santa Barbara, CA, USA; [3]Amherst College, Amherst, MA, USA

Corresponding author: W. F. Hoover (wfhoover@uw.edu)

Key Points:

- Contrasting actinolite microstructures in talc-free and talc-bearing subduction interface metasomatic rocks record stress variations
- Stress amplification in actinolite from talc schist results from high strain rate deformation of surrounding talc
- High strain rates reflect episodic slow slip events localized in talc schist under high pore fluid pressures during active metasomatism

Abstract

Episodic tremor and slow slip (ETS) downdip of the subduction seismogenic zone are poorly understood slip behaviors of the seismic cycle. Talc, a common metasomatic mineral at the subduction interface, is suggested to host slow slip but this hypothesis has not been tested in the rock record. We investigate actinolite microstructures from talc-bearing and talc-free rocks exhumed from the depths of modern ETS (Pimu'nga/Santa Catalina Island, California). Actinolite deformed by dissolution-reprecipitation creep in the talc-free rock and dislocation creep ± cataclasis in the talc-bearing rock. This contrast results from stress amplification in the talc-bearing rock produced by high strain rates in surrounding weak talc. We hypothesize that higher strain rates in the talc-bearing sample represent episodic slow slip, while lower strain rates in the talc-free sample represent intervening aseismic creep. This work highlights the need to consider fluid-mediated chemical change in studies of subduction zone deformation and seismicity.

Plain Language Summary

Episodic tremor and slow slip (ETS) are poorly understood styles of fault slip that occur just below the locked part of the megathrust fault where large subduction zone earthquakes occur. Chemical reactions at the depths of ETS can produce new and particularly weak minerals such as talc that change fault behavior but are rarely considered in studies of ETS. Modeling of rock deformation suggests that talc should host ETS fault slip, but this hypothesis has not been tested in the rock record. We investigated deformation of the mineral actinolite in talc-free and talc-bearing rocks exhumed from the depths of ETS in modern subduction zones on Pimu'nga/Santa Catalina Island (California) as a record of fault slip. Contrasting microstructures and deformation mechanisms in talc-free and talc-bearing rocks are best explained by differences in the rate of deformation (strain rate) between the two rock types. Lower strain rates in talc-free rocks likely record background creeping (aseismic) deformation and higher strain rates in talc-bearing rocks likely represent episodic slow slip events. This work

suggests that talc may be a key host for slow slip and that future studies must account for new rock types formed by chemical reactions to accurately represent subduction zone deformation.

1 Introduction

Slow slip occurs at rates faster than aseismic creep but slower than seismic slip and is observed along the subduction interface below the seismogenic zone (e.g., Beroza & Ide, 2011). When occurring episodically alongside non-volcanic tremor, these phenomena are called episodic tremor and slip (ETS) and represent an integral yet poorly constrained part of the subduction seismic cycle (e.g., Bürgmann, 2018; Obara, 2002; Rogers & Draggert, 2003). Geophysical observations suggest that source regions of ETS are fluid-rich and subject to high pore fluid pressures (e.g., Audet et al., 2009; Delph et al., 2018; Hawthorne & Rubin, 2010; Houston, 2015), consistent with geologic evidence of abundant fluid-rock interaction in rocks exhumed from these regions (e.g., Bebout & Penniston-Dorland, 2016; Condit & French, 2022). Both viscous and frictional deformation mechanisms have been proposed for slow slip, though frictional mechanisms are most consistent with low shear stresses and rheologic constraints (e.g., Condit et al., 2022; French & Zhu, 2017; Hayman & Lavier, 2014; Leeman et al., 2018; Phillips et al., 2020). However, the rheological impact of metasomatic transformation remains underexplored in many proposed mechanisms for slow slip.

Rheological modeling predicts that metasomatic talc-rich, and to a lesser extent chlorite-rich, rocks host slow slip by frictional sliding under elevated pore fluid pressures at low shear stresses (French and Condit, 2019). Talc-rich rocks are common in exhumed paleosubduction interface mélanges where they are interpreted as the result of fluid-mediated reactions between chemically contrasting strong blocks and weak matrix lithologies (e.g., Bebout & Barton, 2002; Bebout & Penniston-Dorland, 2016; Gyomlai et al., 2021; King et al., 2003; Spandler et al., 2008). Talc has a low coefficient of friction and is velocity-strengthening to -neutral, making it a prime candidate to host slow slip if frictional deformation can be activated, and emphasizing the potential rheological impact of metasomatically-produced minerals (Chen et al., 2017; Hirauchi et al., 2020; Misra et al., 2014; Moore & Lockner, 2004; 2008).

Here, we investigate the role of talc in hosting ETS through a microstructural study of talc-bearing and talc-free subduction interface rocks exhumed from the depths of ETS in modern subduction zones (Fig. 1a and b). These rocks display contrasting amphibole microstructures that are best explained by stress amplification resulting from higher strain rates in talc-bearing rocks. These observations are consistent with episodic slow slip accommodated by frictional deformation in talc-bearing metasomatic rocks during periods of elevated pore fluid pressure.

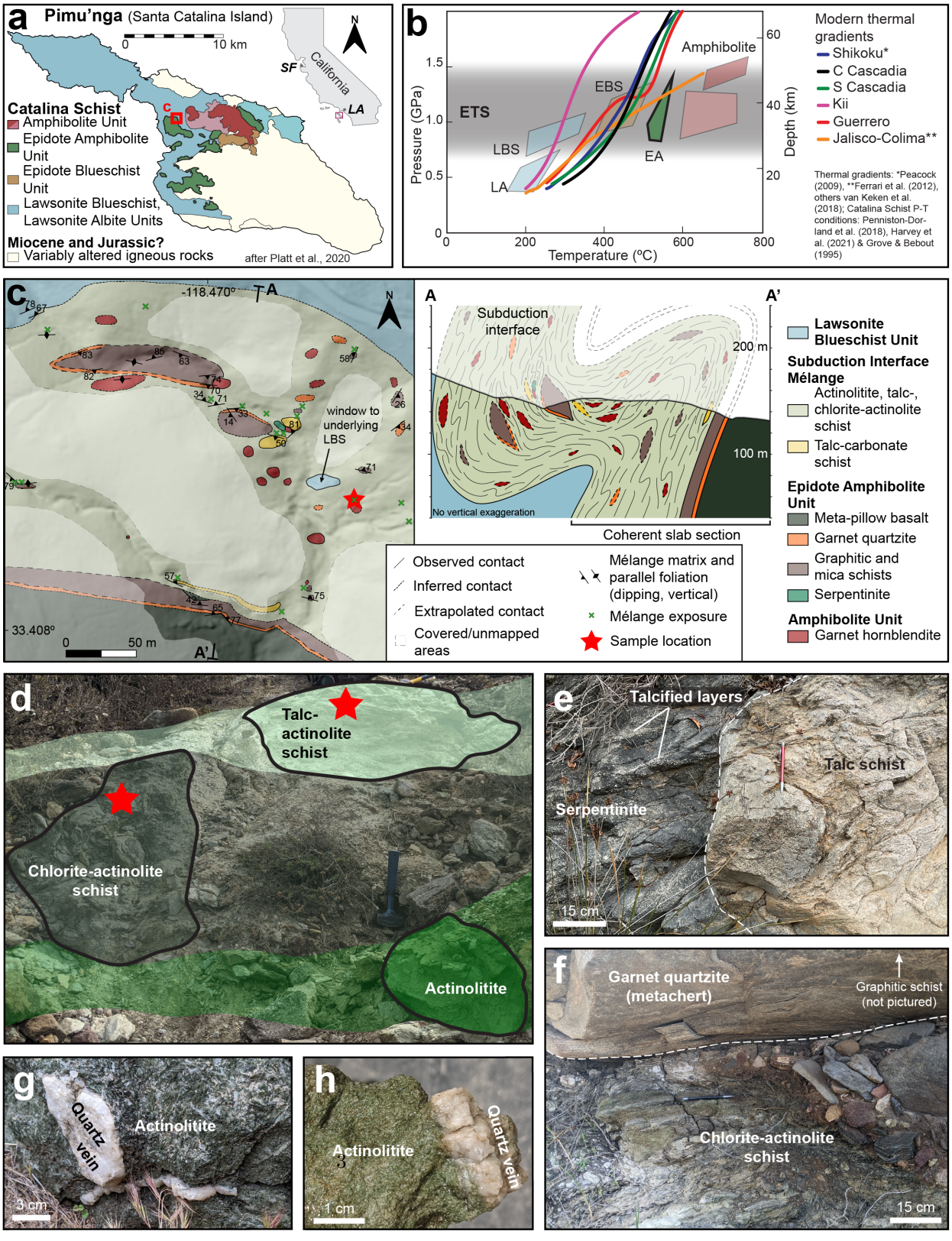
a
Pimu'nga (Santa Catalina Island)
0
10 km
N
SF
California
LA
C
Catalina Schist
Amphibolite Unit
Epidote Amphibolite Unit
Epidote Blueschist Unit
Lawsonite Blueschist, Lawsonite Albite Units
Miocene and Jurassic?
Variably altered igneous rocks
after Platt et al., 2020
b
Amphibolite
EBS
ETS
LBS
EA
LA
Pressure (GPa)
Depth (km)
Temperature (°C)
Modern thermal gradients
Shikoku*
C Cascadia
S Cascadia
Kii
Guerrero
Jalisco-Colima**
Thermal gradients: *Peacock (2009), **Ferrari et al. (2012), others van Keken et al. (2018); Catalina Schist P-T conditions: Penniston-Dorland et al. (2018), Harvey et al. (2021) & Grove & Bebout (1995)
c
-118.470°
33.408°
A
A'
N
window to underlying LBS
0
50 m
Subduction interface
200 m
100 m
No vertical exaggeration
Coherent slab section
Observed contact
Inferred contact
Extrapolated contact
Covered/unmapped areas
Mélange matrix and parallel foliation (dipping, vertical)
Mélange exposure
Sample location
Lawsonite Blueschist Unit
Subduction Interface Mélange
Actinolitite, talc-, chlorite-actinolite schist
Talc-carbonate schist
Epidote Amphibolite Unit
Meta-pillow basalt
Garnet quartzite
Graphitic and mica schists
Serpentinite
Amphibolite Unit
Garnet hornblendite
d
Talc-actinolite schist
Chlorite-actinolite schist
Actinolitite
e
Talcified layers
Talc schist
Serpentinite
15 cm
f
Garnet quartzite (metachert)
Graphitic schist (not pictured)
Chlorite-actinolite schist
15 cm
g
Quartz vein
Actinolitite
3 cm
h
Actinolitite
Quartz vein
1 cm

Figure 1: Geologic context of the studied samples. (a) Geologic map of the Catalina Schist. (b) Pressure-temperature conditions of the Catalina Schist units relative to modern subduction zone thermal gradients and conditions of modern episodic tremor and slip. (c) Map and interpretive cross-section of the sampled mélange separating the Epidote Amphibolite and Lawsonite Blueschist units. (d) Photo of the sampled outcrop showing the variety of metasomatic lithologies and inferred structural relationships (hammer for scale). (e) Photo of nearby talc schist in contact with serpentinite. (f) Photo of nearby chlorite-actinolite schist in contact with an Epidote Amphibolite metasedimentary sequence. (g and h) Field and hand sample photos of quartz veins in nearby actinolitite.

2 Geologic background

The Catalina Schist is an exhumed paleosubduction terrane exposed on Pimu'nga/Santa Catalina Island (California) and composed of units preserving variable depths and thermal gradients along the subduction interface (Fig. 1a; Platt, 1975). Peak temperature, pressure, and age decrease from the structurally highest to lowest units (Fig. 1b; Grove & Bebout, 1995; Harvey et al., 2021; Penniston-Dorland et al., 2018; Platt, 1975; Sorensen, 1986). Mélange zones in all units have been interpreted as paleosubduction interfaces formed through progressive metasomatism and mechanical mixing of block and matrix lithologies (e.g., Bebout & Barton, 1989; Bebout & Barton, 2002; King et al., 2006; Penniston-Dorland et al., 2014; Sorensen & Barton, 1987; Sorensen & Grossman, 1989). The samples studied here were collected from a mélange zone separating the Lawsonite Blueschist (LBS) and Epidote Amphibolite (EA) units which reached peak metamorphic conditions of 200-350^{o}C, 0.7-1.0 GPa and 500-550^{o}C and 0.7-1.4 GPa, respectively (Fig. 1b; Grove & Bebout, 1995). These conditions overlap with those inferred for ETS in active subduction zones (e.g., Condit et al., 2020; Fig. 1b).

3 Field context

The sampled mélange zone and adjacent LBS and EA were mapped to contextualize the microstructural observations (Fig. 1c). Both the EA and LBS are composed of coherent seafloor lithostratigraphy containing meta-(pillow) basalts, metachert (garnet quartzite), and metasedimentary schists (Platt, 1976). The intervening mélange zone, ~100 m thick, contains blocks of EA metasedimentary rocks (metachert, graphitic and mica schists) and variably altered garnet hornblendite in a metasomatized matrix (Fig. 1c). No blocks of any LBS lithology were found in the mélange zone. The metasomatic mélange matrix is dominated by layers of talc and chlorite schists and actinolitite from 10s to 100s of cm thick (Fig. 1d-f). Talc schist is in contact with a serpentinite block and chlorite schist is in contact with blocks of graphitic schist and metachert (Fig. 1e and f). Coherent layering in the mélange matrix is traceable up to ~100 m. Multiple orientations of quartz veins are commonly observed cross-cutting actinolitite (Fig. 1g and h). Representative samples of the chlorite- and talc-bearing mélange matrix were collected from a single outcrop to investigate their

microstructures (Fig. 1d).

4 Samples and microstructures

4.1 Chlorite-actinolite schist

The chlorite schist has a strong foliation defined by mm- to cm-scale layering of chlorite- and actinolite-rich domains. Microstructure and modal mineralogy are highly variable, but the dominant assemblage is chlorite, actinolite and graphite and minor rutile, titanite, apatite, and talc (<1%). A cm-thick chlorite layer is made up of large (~750 m) interlocking chlorite plates that are radially oriented and exhibit kinking and undulose extinction (Fig. 2a). The boundaries of this radial chlorite layer are sharp with chlorite plates truncated against highly aligned actinolite ± chlorite rather than rotated into the foliation (Fig. 2a). A large (1.5 mm) actinolite grain growing across this boundary is broken and rotated into the neighboring actinolite ± chlorite foliation (Fig. 2b). Adjacent to the radial-chlorite layer are highly deformed actinolite ± chlorite domains. These domains have reduced chlorite grain size and a strong foliation defined by aligned chlorite cleavage planes (Fig. 2c), while actinolite-only domains have elongate to acicular textures (Fig. 2a). Away from the radial-chlorite layer, actinolite domains range in texture from equant to elongate with relict composite fabrics discordant to the dominant foliation (Fig. 2d).

4.3 Talc-actinolite schist

The talc schist is composed of talc and actinolite with minor chlorite and inclusions of Cr-spinel in actinolite. This sample has weak compositional layering of talc- and actinolite-rich domains and a strong foliation defined by alignment of both talc and actinolite. In talc-rich domains, foliation is defined by near-uniformly oriented talc cleavage planes and aligned actinolite porphyroclasts and aggregates (Fig. 2e). In actinolite-rich domains, actinolite ranges from porphyroclastic to acicular in texture. Actinolite porphyroclasts and aggregates show distinct fracturing and disaggregation along basal cleavage planes in all domains (Fig. 2f).

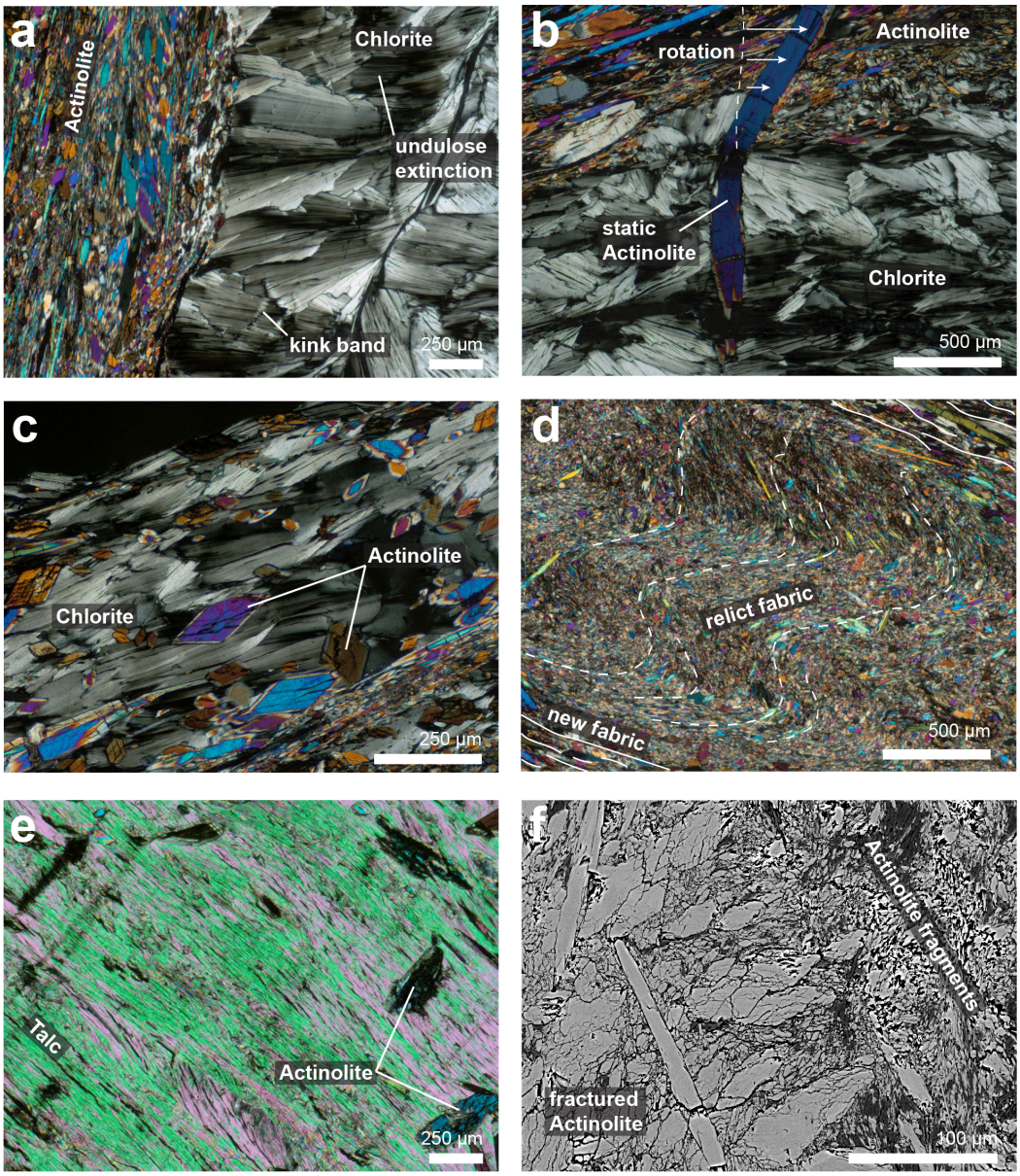

Figure 2: Cross-polarized light photomicrographs (a-e) and a back-scattered electron image (f) of microstructures. Chlorite-actinolite schist: (a) Contrast between the highly strained actinolite (±chlorite) domain and relatively undeformed radial chlorite layer. (b) Rotation of actinolite statically grown across the radial chlorite layer boundary. (c) Partitioning of deformation into chlorite

in a mixed-mineral domain. (d) Relict fabric in metasomatic actinolite overprinted by current foliation. Talc-actinolite schist: (e) Highly aligned and heavily sheared talc with actinolite porphyroclasts. (f) Comminution of fractured actinolite porphyroclasts to a groundmass of actinolite fragments.

5 Compositional Zoning and Textural Data

5.1 Methods

A Thermo-Fisher/FEI Apreo-S scanning electron microscope equipped with an Oxford Instruments Symmetry electron backscatter diffraction detector and Ultim-Max 100 energy dispersive spectroscopy detector was used to map actinolite composition and crystallographic orientation. Analytical conditions and full data set are provided in the Supplementary Information.

5.2 Actinolite composition and zonation

Amphibole compositions overlap in both samples and all fall within the fields of actinolite, tremolite, and magnesio-hornblende (Supplementary Data; Leake et al., 1997). In the chlorite-actinolite schist, oscillatory zoning in Al, Fe and Na is often truncated by grain boundaries (Fig. 3c and d). In the talc-actinolite schist, Cr and Al are enriched in concentric porphyroclast rims, along fractures, and in domains of grain size reduction (Fig. 3e and f).

5.3 Quantitative analysis of actinolite microstructures

In the talc-free sample (chlorite-actinolite schist), intragrain misorientation in actinolite is minimal with ~80% of misorientations $<1^{o}$ (Fig. 3a and g). In the talc-actinolite schist, amphibole grains exhibit abundant intragrain misorientations with ~70% of misorientations $>1^{o}$ (Fig. 3a and g). In the talc-actinolite schist misorientation gradients and subgrains are common, with the latter often developed along amphibole cleavage planes (Fig. 3a). No difference was observed between actinolite microstructures in actinolite-rich versus sheet silicate-rich domains within either sample (Fig. 3). Both talc- and chlorite-rich samples have strong actinolite CPOs with [001] point maxima within the foliation, and dominantly [100] point maxima perpendicular to the foliation with less frequent [100] girdles (Fig. 3b). The orientations of [001] point maxima vary between textural domains suggesting multiple deformation mechanisms or fabrics (Fig. 3b).

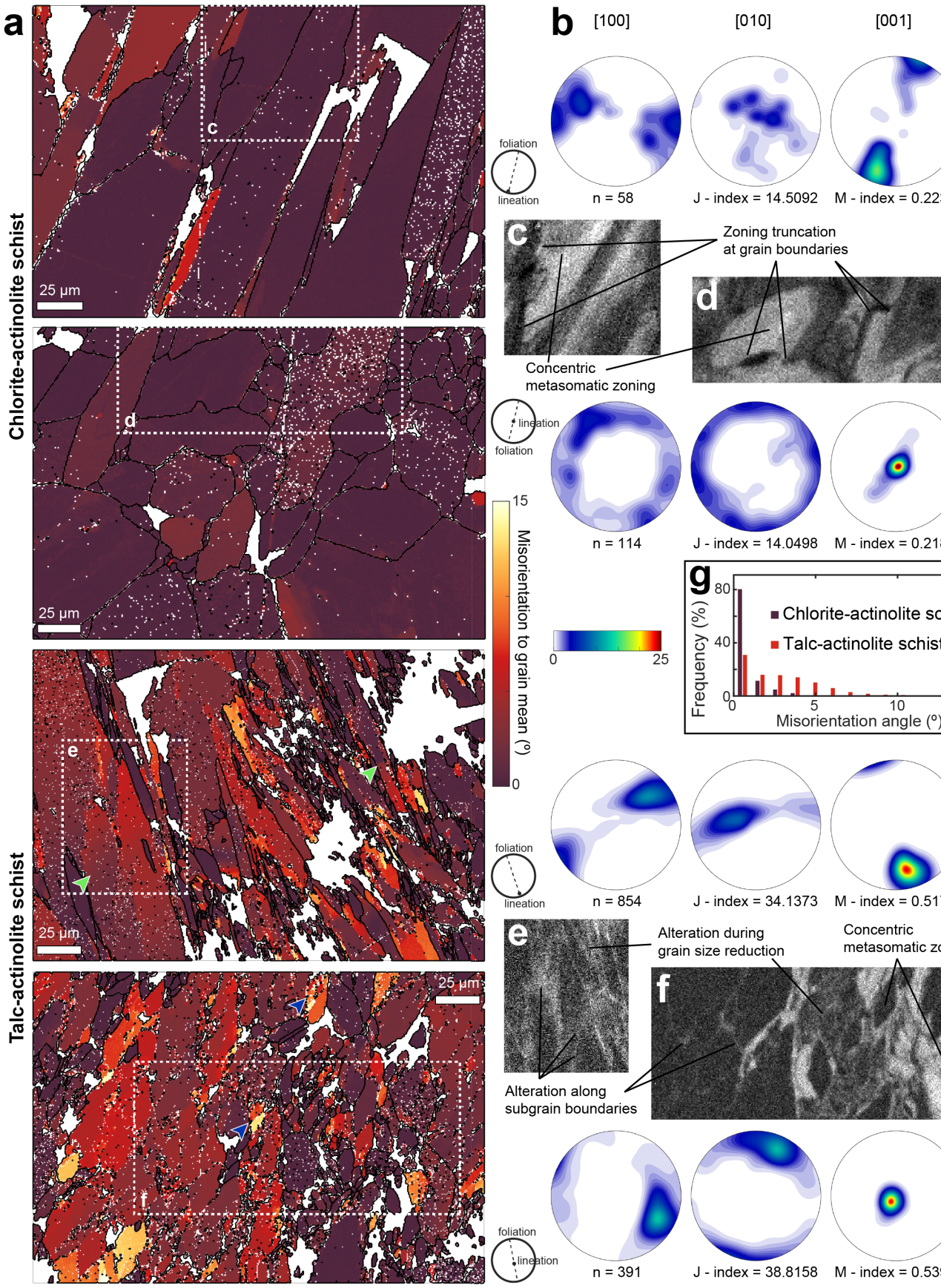
a
Chlorite-actinolite schist
Talc-actinolite schist
25 µm
c
d
e
f
b
[100]
[010]
[001]
foliation
lineation
n = 58
J - index = 14.5092
M - index = 0.22
Zoning truncation
at grain boundaries
Concentric
metasomatic zoning
n = 114
J - index = 14.0498
M - index = 0.21
15
0
Misorientation to grain mean (°)
0
25
g
Frequency (%)
80
40
0
Chlorite-actinolite sc
Talc-actinolite schist
0
5
10
Misorientation angle (°)
n = 854
J - index = 34.1373
M - index = 0.51
Alteration during
grain size reduction
Concentric
metasomatic zo
Alteration along
subgrain boundaries
n = 391
J - index = 38.8158
M - index = 0.53

Figure 3: Electron back-scatter diffraction data showing contrasting microstructures in talc-free (top) and talc-bearing samples (bottom). (a) Maps of the pixel misorientation to the grain mean for actinolite showing limited intragrain misorientation in the talc-free sample contrasting with extensive intragrain misorientation gradients (green arrows) and subgrain formation (blue arrows) in the talc-bearing sample. (b) Crystallographic preferred orientation of actinolite. (c-f) Aluminum chemical map insets from (a) showing zonation truncated at grain boundaries in the chlorite-actinolite schist (c-d) and chemical modification along subgrain boundaries (e) and grain-size-reduced domains (f) in the talc-actinolite schist. (g) Histogram of actinolite misorientation angle showing higher abundance and angle of misorientations in talc-bearing rocks.

6 Discussion

6.1 Subduction interface mélange setting

The mapped mélange zone is characterized by a block-in-matrix texture and occurrence of hybrid lithologies comparable to other subduction interface mélanges of the Catalina Schist (e.g., Bebout & Barton, 1989; Sorensen & Barton, 1987). The absence of LBS lithologies in the mélange suggest it underwent limited deformation or mélange formation after EA peak metamorphic conditions (Fig. 1c). The position of the studied mélange above EA seafloor lithostratigraphy corroborates its origin as a paleosubduction interface formed above the coherent EA slab section (Fig. 1c). Field relationships suggest that the talc-actinolite schist and chlorite-actinolite schist formed from ultramafic and sedimentary protoliths, respectively, likely representing the reaction between overriding mantle wedge and downgoing slab sediments (Fig. 1e and f). Overprinting relationships between mineral zonation and deformation fabrics indicate that metasomatism and deformation of the mélange were concurrent (Fig. 2b and d, 3a, c-f). Together, the pressure-temperature conditions of formation, subduction interface setting, and co-occurring deformation and metasomatism of this mélange are ideal for investigating processes at the depths of ETS in modern subduction zones like Shikoku, Mexico, and Cascadia (Fig. 1b; e.g., Condit et al., 2020).

6.2 Contrasting talc and chlorite deformation

Talc and chlorite are both considered "weak" minerals but exhibit contrasting microstructures in these samples (e.g., Moore & Lockner, 2008; Okamoto et al., 2019). Talc cleavage planes are near-uniformly aligned in the talc-actinolite schist, suggesting talc may have accommodated significant strain by frictional sliding along [001] (e.g., Moore & Lockner, 2008; Fig. 2e). In contrast, the ability of chlorite to accommodate high strain appears to have been highly dependent on orientation and phase mixing. In the radial-chlorite layer in the chlorite-actinolite schist, large, interlocking, radial plates of chlorite exhibit kinking and undulose extinction (Fig. 2a). Given that dislocation glide and frictional sliding in chlorite are both reliant on the alignment of [001] planes, these microstructures are consistent with strain hardening due to unfavorable mineral alignment and a lack of recovery mechanisms (e.g., Okamoto et al.,

2019). These microstructures suggest that the chlorite layer acted as a strong body that localized deformation into adjacent actinolite and actinolite + chlorite domains. Only in mixed actinolite + chlorite domains did chlorite grain size remain small, potentially facilitating reorientation and alignment of [001] to accommodate significant strain (Fig. 2c). These microstructural contrasts between talc and chlorite highlight the complexity of sheet silicate deformation and the importance of orientation, texture, and grain size in determining their strength, often in contrast with constitutive relations (e.g., chlorite; Okamoto et al., 2019).

6.3 Stress variations in actinolite

Actinolite shares similar compositional ranges and textures in both rocks yet exhibits strongly contrasting microstructures between rocks with or without volumetrically significant talc (>1%; Fig. 3). In the talc-free sample, limited intragrain deformation and the truncation of chemical zoning at grain boundaries suggests dissolution-reprecipitation creep as the dominant deformation mechanism in actinolite (Fig. 3; e.g., Giuntoli et al., 2018; Imon et al., 2004; Lee et al., 2022; Condit & Mahan, 2018; Soret et al., 2019). The strong CPO in this sample with [100] oriented perpendicular to the foliation suggests an additional contribution from rigid body rotation (Fig. 3b; Berger & Stunitz, 1996; Getsinger & Hirth, 2014). Dissolution-reprecipitation creep is a commonly observed deformation mechanism in natural and experimental amphibole (e.g., Berger & Stunitz, 1996; Condit & Mahan, 2018; Getsinger & Hirth, 2014; Imon et al., 2004; Lee et al., 2022). This mechanism has been reported in a range of amphibole compositions and P-T conditions and would be expected given the low stresses and abundant fluids in this subduction interface setting (e.g., Bebout & Penniston-Dorland, 2016; Behr & Platt, 2013; Condit et al., 2022; Wassman & Stöckert, 2013).

In contrast, in the talc-bearing sample, intragrain deformation of actinolite is abundant with the development of misorientation gradients and subgrains, a strong CPO (Fig. 3), and petrographically observed fracturing and disaggregation of actinolite porphyroclasts (Fig. 2f). These microstructures are scale-invariant between single actinolite crystals surrounded by talc, mm-scale actinolite aggregates in talc, and cm-scale actinolite-rich domains. Based on these microstructures, actinolite in the talc-bearing sample was dominantly deformed via dislocation creep with or without cataclasis (e.g., Babaie & La Tour, 1994; Imon et al., 2004; Soret et al., 2019). While cataclasis has been reported in many previous studies of amphibole deformation, dislocation creep is rare and has been associated with dry conditions, high temperatures, and high stresses and strain rates (e.g., Brückner & Trepmann, 2021; Diaz Aspiroz et al., 2007; Hacker & Christie, 1990; Soret et al., 2019). Thus, the actinolite microstructures observed in the talc-bearing sample are unusual because of the activation of dislocation creep at relatively low temperature, under fluid-rich conditions, and in the presence of weak talc.

For minerals with well-mapped deformation mechanisms such as quartz, olivine,

and feldspar, the shift from dissolution-reprecipitation creep to dislocation creep is produced by an increase in stress, holding other variables constant (e.g., Goetze, 1978; Rutter & Brodie, 2004; Rybacki & Dresen, 2004). Amphibole deformation mechanisms are poorly constrained in pressure-temperature-stress-fluid-grain size-composition space and clearly complex, but the little published experimental deformation of amphibole revealed plastic deformation was activated at high stresses and strain rates (e.g., Brückner & Trepmann, 2021; Hacker & Christie, 1990; Rooney et al., 1975). In this framework, the observed actinolite microstructures are best explained by higher stresses experienced by actinolite in the talc-bearing sample compared to the talc-free sample. Given the overlapping amphibole composition, grain size, and a shared pressure-temperature-fluid history for these adjacent mélange matrix samples, local stress variations are the most likely explanation for the microstructural contrast.

6.4 Strain rate variations and slow slip

Local stress variations can occur in two-phase mixtures depending on the strength contrast between phases and the abundance of strong clasts versus weak matrix (e.g., Handy, 1990). For moderate clast fractions (>0.3), "jamming" of clasts creates load-bearing force chains that amplify clast stresses by 2-14x, depending on clast-matrix strength contrast (Beall et al., 2019a; 2019b; Cates et al., 1998; Webber et al., 2018). Even at low clast fractions (<0.1) and in the absence of clast-clast interaction, clast stress shadows, and the matrix itself, can impose stress on clasts resulting in stress amplification of 2-5x that on the matrix (Ioannidi et al., 2022; Ladd & Reber, 2020). These numerical models, experiments and geologic studies are scale independent, and are consistent with the microstructures observed here reflecting stress amplification in strong actinolite due to force-chain formation and/or stress transfer from the weak talc matrix.

Actinolite stress amplification is absent from the chlorite-actinolite schist despite similar or greater actinolite abundances, suggesting stress amplification is controlled by matrix mineralogy and its orientation. Actinolite grains are juxtaposed in force chains by matrix strain, and stress transferred from weak to strong phase undergoes time-dependent relaxation, so in both cases higher strain rates result in increased efficiency of stress amplification (e.g., Beall et al., 2019a; Ladd & Reber, 2020). Clast stress amplification is also dependent on clast-matrix viscosity contrast, so lower viscosity of talc relative to chlorite (or misalignment of chlorite [001]) could explain stress amplification only in the talc-bearing rock and would yield higher strain rates in talc (e.g., Beall et al., 2019a; Fagereng & Sibson, 2010; Moore & Lockner, 2008; Okamoto et al., 2019). Thus, multiple lines of reasoning suggest stress amplification in the talc-bearing sample and its absence in the talc-free sample reflects higher strain rates accommodated by weaker talc.

In this rheological model, variations in stresses experienced by actinolite act as a key microstructural recorder of higher strain rates accommodated by talc deformation relative to chlorite or actinolite in the chlorite-actinolite schist. This

interpretation is consistent with the prediction that talc will partition high-strain-rate deformation via frictional sliding during slow slip at high pore fluid pressures (French & Condit, 2019). The uniform alignment of talc cleavage planes observed in the talc-bearing sample would enable this frictional mechanism, though diagnostic microstructures for frictional sliding in talc are poorly constrained. In this model, lower stress and strain rate deformation of actinolite and chlorite in talc-free rocks occurred during periods of slower deformation (aseismic creep), while high strain rate deformation of talc-rich rocks occurred during slow slip events (Fig. 4).

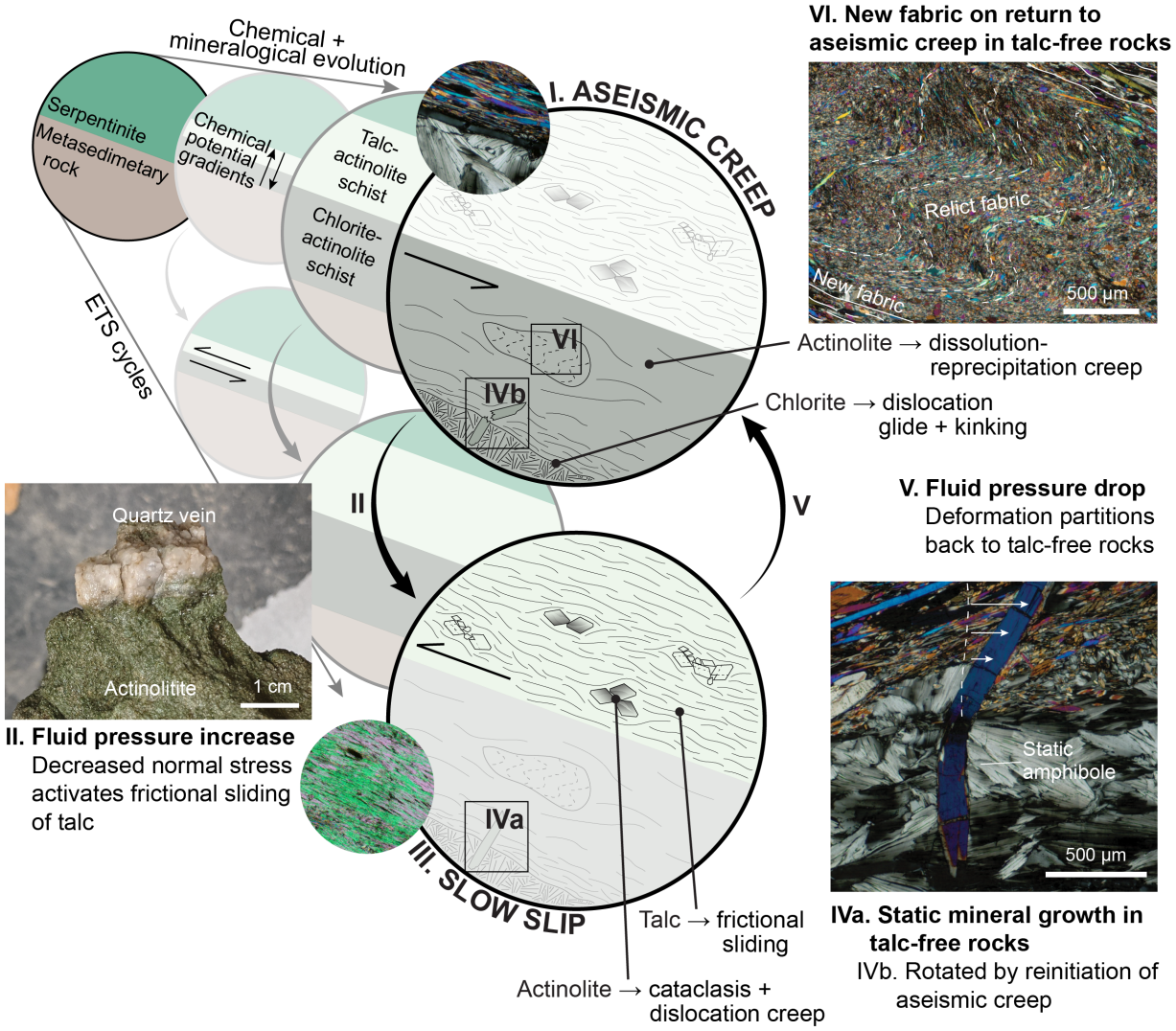

Figure 4: Conceptual model for the evolution of the observed microstructures

during episodic tremor and slip. During background aseismic creep deformation is partitioned into talc-free metasomatic rocks (I). During slow slip, fluid pressure increase (II) activates frictional sliding in talc (III) and high strain rates juxtapose actinolite producing local stress amplification. During slow slip events, the cessation of deformation allows the growth of static minerals in talc-free rocks (IVa) that are later rotated when fluid pressure drops (IVb and V), and aseismic creep is resumed (I). Episodic deformation leads to the develop of complex microstructures characterized by multiple overprinting fabrics in chlorite-actinolite schist (VI).

6.5 Comparison to rheological modelling and ETS

Partitioning of slow slip deformation into talc is hypothesized from rheological modeling when pore fluid pressures are high enough to activate frictional sliding (French & Condit, 2019). The development of the metasomatic talc-rich lithologies studied here is the direct result of abundant fluids that catalyzed and mediated chemical reactions (e.g., Bebout & Barton, 2002). In addition, the quartz veins in adjacent actinolitite suggest periods of high pore fluid pressures in this already fluid-rich environment, consistent with evidence of high fluid pressures in modern and exhumed subduction interfaces (Fig. 1g and h; Audet et al., 2009; Condit & French, 2022; Kodaira et al., 2004; Raimbourg et al., 2022). Thus, in this mélange zone, the fluid pressure conditions of the rheological model for frictional deformation of talc are likely met, consistent with our interpretation that high strain rates in the talc-bearing sample may represent slow slip events.

Episodic slow slip in this suite of talc-free and talc-bearing rocks would be expected to produce a record of alternating aseismic creep and slow slip deformation. Here again, microstructures corroborate our interpretation that these rocks record episodic slow slip. In the chlorite-actinolite schist, lenses of metasomatic actinolite preserve relict fabrics recording earlier episodes of syn-reaction deformation (Fig. 4). Likewise, the growth, and later rotation, of a large actinolite crystal across the boundary between an actinolite layer and the radial-chlorite layer indicates a cessation and reinitiation of deformation at this boundary (Fig. 4). These textures provide direct evidence of episodic static and dynamic conditions in the chlorite-actinolite schist consistent with periodic partitioning of deformation into the talc-actinolite schist during slow slip controlled by pore fluid pressure magnitude and matrix strength.

6.6 Implications for ETS

We show here that talc-bearing rocks may have hosted episodic slow slip events in a paleosubduction zone. Constitutive relations, deformation experiments and geologic studies suggest talc may be a ubiquitous host of deep slow slip (e.g., French & Condit, 2019; Moore & Lockner, 2008; Spandler et al., 2008). Talc is stable from seafloor to subarc conditions, is common in exhumed paleosubduction interfaces from a variety of depths and is formed by reaction between Si- and Mg-rich rocks (e.g., Bose & Ganguly, 1995; D'Orazio et al., 2004; Kim

et al., 2010; Spandler et al., 2008). Juxtaposition of these rock types is most prevalent below the seismogenic zone (i.e., mantle wedge corner) where talc could host all deep episodic slow slip, but the broad stability, rheology, and ubiquity of metasomatic minerals, talc, and in its absence, chlorite, could make them important contributors to slow slip at a range of depths. Multiple lines of evidence for talc as the host of slow slip indicate a causal relationship between metasomatism and the rheological preconditions for slow slip. Metasomatism, and not closed system metamorphism, is required to produce these minerals capable of hosting deep slow slip. In light of this work, it is imperative that studies of deformation in subduction zones consider not only subduction zone inputs and their metamorphosed equivalents, but equally the hybrid lithologies produced by chemical reactions (e.g., talc and chlorite schists; e.g., Phillips et al., 2020). Ignoring these lithologies will result in spurious conclusions on the strength of the subduction interface and the host(s) of slow slip.

7 Conclusions

We document evidence of stress and strain rate variations in actinolite microstructures from subduction interface metasomatic rocks exhumed from the pressure-temperature conditions of modern episodic tremor and slow slip. Evidence for dislocation creep/cataclasis in the talc-bearing rock and dissolution-reprecipitation creep in the talc-free rock reflects variable stresses. Higher stresses in actinolite from the talc-bearing sample reflect stress amplification during high strain rate deformation of the surrounding talc. Along with evidence from rheological modeling, the presence of quartz veins and textural evidence of episodic deformation, these strain rate variations are interpreted to reflect episodic high strain rates during slow slip events in the talc-bearing sample with lower strain rates in the talc-free sample during intervening aseismic creep. This work demonstrates the importance of considering metasomatism in studying subduction zone seismicity and its likely role in episodic tremor and slow slip.

Acknowledgements

These samples were collected on unceded lands of the Gabrielino-Tongva and we offer this Land Acknowledgement to affirm their ongoing sovereignty in the face of settler-colonialism and as a commitment to support and advocate for equitable research on their lands. We thank the Santa Catalina Island Conservancy for support with sample collection. This work was funded by NSF EAR-2053033 to Hoover. John Platt is thanked for introducing the authors to the field area and for discussions of field mapping. We thank M.E. French, A. Kotowski, C. Seyler, S. Penniston-Dorland and the attendees at the Penrose Conference on Slow Earthquakes for insightful discussion.

Open Research

The microstructural and geochemical data presented in this paper are available in the Supplementary Information. Data was processed using the open-source MTEX (v. 5.7.0) MATLAB toolbox.

References

Audet, P., Bostock, M. G., Christensen, N. I., & Peacock, S. M. (2009). Seismic evidence for overpressured subducted oceanic crust and megathrust fault sealing. *Nature*, *457*(7225), 76–78. https://doi.org/10.1038/nature07650

Babaie, H. A., & La Tour, T. E. (1994). Semibrittle and cataclastic deformation of hornblende-quartz rocks in a ductile shear zone. *Tectonophysics*, *229*(1–2), 19–30. https://doi.org/10.1016/0040-1951(94)90003-5

Bachmann, F., Hielscher, R., & Schaeben, H. (2010). Texture analysis with MTEX - Free and open source software toolbox. *Solid State Phenomena*, *160*, 63–68.

Beall, A., Fagereng, Å., & Ellis, S. (2019a). Fracture and Weakening of Jammed Subduction Shear Zones, Leading to the Generation of Slow Slip Events. *Geochemistry, Geophysics, Geosystems*, *20*, 4869–4884. https://doi.org/10.1029/2019GC008481

Beall, A., Fagereng, Å., & Ellis, S. (2019b). Strength of Strained Two-Phase Mixtures: Application to Rapid Creep and Stress Amplification in Subduction Zone Mélange. *Geophysical Research Letters*, *46*(1), 169–178. https://doi.org/10.1029/2018GL081252

Bebout, G. E., & Barton, M. D. (1989). Fluid flow and metasomatism in a subduction zone hydrothermal system: Catalina Schist terrane, California. *Geology*, *17*(11), 976–980. https://doi.org/10.1130/0091-7613(1989)017<0976:FFAMIA>2.3.CO;2

Bebout, G. E., & Barton, M. D. (2002). Tectonic and metasomatic mixing in a high-T, subduction-zone mélange — insights into the geochemical evolution of the slab – mantle interface. *Chemical Geology*, *187*, 79–106.

Bebout, G. E., & Penniston-Dorland, S. C. (2016). Fluid and mass transfer at subduction interfaces - The field metamorphic record. *Lithos*, *240–243*, 228–258. https://doi.org/10.1016/j.lithos.2015.10.007

Behr, W. M., & Platt, J. P. (2013). Rheological evolution of a Mediterranean subduction complex. *Journal of Structural Geology*, *54*(c), 136–155. https://doi.org/10.1016/j.jsg.2013.07.012

Berger, A., & Stünitz, H. (1996). Deformation mechanisms and reaction of hornblende: Examples from the Bergell tonalite (Central Alps). *Tectonophysics*, *257*(2-4 SPEC. ISS.), 149–174. https://doi.org/10.1016/0040-1951(95)00125-5

Beroza, G. C., & Ide, S. (2011). Slow Earthquakes and Nonvolcanic Tremor. *Annual Review of Earth and Planetary Sciences*, *39*(1), 271–296. https://doi.org/10.1146/annurev-earth-040809-152531

Bose, K., & Ganguly, J. (1995). Experimental and theoretical studies of the stabilities of talc, antigorite and phase A at high pressures with applications to subduction processes. *Earth and Planetary Science Letters*, *136*(95), 109–121.

Brückner, L. M., & Trepmann, C. A. (2021). Stresses during pseudotachylyte formation - Evidence from deformed amphibole and quartz in fault rocks from the Silvretta basal thrust (Austria). *Tectonophysics*, *817*(June), 229046. https://doi.org/10.1016/j.tecto.2021.229046

Bürgmann, R. (2018). The geophysics, geology and mechanics of slow fault slip. *Earth and Planetary Science Letters*, *495*, 112–134. https://doi.org/10.1016/j.epsl.2018.04.062

Cates, M. E., Wittmer, J. P., Bouchaud, J. P., & Claudin, P. (1998). Jamming, force chains, and fragile matter. *Physical Review Letters*, *81*(9), 1841–1844. https://doi.org/10.1103/PhysRevLett.81.1841

Chen, X., Elwood Madden, A. S., & Reches, Z. (2017). The frictional strength of talc gouge in high-velocity shear experiments. *Journal of Geophysical Research: Solid Earth*, *122*(5), 3661–3676. https://doi.org/10.1002/2016JB013676

Condit, C. B., & French, M. E. (2022). Geologic evidence of lithostatic pore fluid pressures the base of the subduction seismogenic zone. *Geophysical Research Letters*. https://doi.org/10.1029/2022gl098862

Condit, Cailey B., & Mahan, K. H. (2018). Fracturing, fluid flow and shear zone development: Relationships between chemical and mechanical processes in Proterozoic mafic dykes from southwestern Montana, USA. *Journal of Metamorphic Geology*, *36*(2), 195–223. https://doi.org/10.1111/jmg.12289

Condit, Cailey B., Guevara, V. E., Delph, J. R., & French, M. E. (2020). Slab dehydration in warm subduction zones at depths of episodic slip and tremor. *Earth and Planetary Science Letters*, *552*, 116601. https://doi.org/10.1016/j.epsl.2020.116601

Condit, Cailey B., French, M. E., Hayles, J. A., Yeung, L. Y., Chin, E. J., & Lee, C. A. (2022). Rheology of metasedimentary rocks at the base of the subduction seismogenic zone. *Geochemistry, Geophysics, Geosystems*, 1–32. https://doi.org/10.1029/2021gc010194

D'Orazio, M., Boschi, C., & Brunelli, D. (2004). Talc-rich hydrothermal rocks from the St. Paul and Conrad fracture zones in the Atlantic Ocean. *European Journal of Mineralogy*, *16*(1), 73–83. https://doi.org/10.1127/0935-1221/2004/0016-0073

Delph, J. R., Levander, A., & Niu, F. (2018). Fluid Controls on the Heterogeneous Seismic Characteristics of the Cascadia Margin. *Geophysical Research Letters*, *45*(20), 11,021-11,029. https://doi.org/10.1029/2018GL079518

Díaz Aspiroz, M., Lloyd, G. E., & Fernández, C. (2007). Development of lattice preferred orientation in clinoamphiboles deformed under low-pressure metamorphic conditions. A SEM/EBSD study of metabasites from the Aracena metamorphic belt (SW Spain). *Journal of Structural Geology*, *29*(4), 629–645. https://doi.org/10.1016/j.jsg.2006.10.010

Fagereng, Å., & Sibson, R. H. (2010). Mélange rheology and seismic style. *Geology*, *38*(8), 751–754. https://doi.org/10.1130/G30868.1

French, M. E., & Condit, C. B. (2019). Slip partitioning along an idealized subduction plate boundary at deep slow slip conditions. *Earth and Planetary Science Letters*, *528*, 115828. https://doi.org/10.1016/j.epsl.2019.115828

French, M. E., & Zhu, W. (2017). Slow fault propagation in serpentinite under conditions of high pore fluid pressure. *Earth and Planetary Science Letters*, *473*, 131–140. https://doi.org/10.1016/j.epsl.2017.06.009

Getsinger, A. J., & Hirth, G. (2014). Amphibole fabric formation during diffusion creep and the rheology of shear zones. *Geology*, *42*(6), 535–538. https://doi.org/10.1130/G35327.1

Giuntoli, F., Menegon, L., & Warren, C. J. (2018). Replacement reactions and deformation by dissolution and precipitation processes in amphibolites. *Journal of Metamorphic Geology*, (December 2017), 1263–1286. https://doi.org/10.1111/jmg.12445

Goetze, C. (1978). The mechanisms of creep in olivine. *Philosophical Transactions of the Royal Society of London. Series A, Mathematical and Physical Sciences*, *288*(1350), 99–119. https://doi.org/10.1098/rsta.1978.0008

Grove, M., & Bebout, G. E. (1995). Cretaceous tectonic evolution of coastal southern California: Insights from the Catalina Schist. *Tectonics*, *14*(5), 1290–1308.

Gyomlai, T., Agard, P., Marschall, H. R., Jolivet, L., & Gerdes, A. (2021). Metasomatism and deformation of block-in-matrix structures in Syros: The role of inheritance and fluid-rock interactions along the subduction interface. *Lithos*, *386–387*, 105996. https://doi.org/10.1016/j.lithos.2021.105996

Hacker, B. R., & Christie, J. M. (1990). Brittle/ductile and plastic/cataclastic transitions in experimentally deformed and metamorphosed amphibolite. *Geophysical Monograph*.

Handy, M. R. (1990). The solid-state flow of polymineralic rocks. *Journal of Geophysical Research*, *95*(B6), 8647–8661. https://doi.org/10.1029/JB095iB06p08647

Harvey, K. M., Penniston-Dorland, S. C., Kohn, M. J., Piccoli, P. M., Penniston-Dorland, S. C., Kohn, M. J., & Piccoli, P. M. (2021). Assessing P-T variability in mélange blocks from the Catalina Schist: Is there differential movement at the subduction interface? *Journal of Metamorphic Geology*, *39*(3), 271–295. https://doi.org/10.1111/jmg.12571

Hawthorne, J. C., & Rubin, A. M. (2010). Tidal modulation of slow slip in Cascadia. *Journal of Geophysical Research: Solid Earth*, *115*(9), 1–15. https://doi.org/10.1029/2010JB007502

Hayman, N. W., & Lavier, L. L. (2014). The geologic record of deep episodic tremor and slip. *Geology*, *42*(3), 195–198. https://doi.org/10.1130/G34990.1

Hirauchi, K. ichi, Yamamoto, Y., den Hartog, S. A. M., & Niemeijer, A. R. (2020). The role of metasomatic alteration on frictional properties of subduction thrusts: An example from a serpentinite body in the Franciscan Complex, California. *Earth and Planetary Science Letters*, *531*, 115967. https://doi.org/10.1016/j.epsl.2019.115967

Houston, H. (2015). Low friction and fault weakening revealed by rising sensitivity of tremor to tidal stress. *Nature Geoscience*, *8*(5), 409–415. https://doi.org/10.1038/ngeo2419

Imon, R., Okudaira, T., & Kanagawa, K. (2004). Development of shape- and lattice-preferred orientations of amphibole grains during initial cataclastic deformation and subsequent deformation by dissolution-precipitation creep in amphibolites from the Ryoke metamorphic belt, SW Japan. *Journal of Structural Geology*, *26*(5), 793–805. https://doi.org/10.1016/j.jsg.2003.09.004

Ioannidi, P. I., Bogatz, K., & Reber, J. E. (2022). The Impact of Matrix Rheology on Stress Concentration in Embedded Brittle Clasts. *Geochemistry, Geophysics, Geosystems*, *23*(3), 1–19. https://doi.org/10.1029/2021GC010127

Kim, Y., Clayton, R. W., & Jackson, J. M. (2010). Geometry and seismic properties of the subducting Cocos plate in central Mexico. *Journal of Geophysical Research: Solid Earth*, *115*(6), 1–22. https://doi.org/10.1029/2009JB006942

King, R. L., Kohn, M. J., & Eiler, J. M. (2003). Constraints on the petrologic structure of the subduction zone slab-mantle interface from Franciscan Complex exotic ultramafic blocks. *Bulletin of the Geological Society of America*, *115*(9), 1097–1109. https://doi.org/10.1130/B25255.1

King, R. L., Bebout, G. E., Moriguti, T., & Nakamura, E. (2006). Elemental mixing systematics and Sr-Nd isotope geochemistry of mélange formation: Obstacles to identification of fluid sources to arc volcanics. *Earth and Planetary Science Letters*, *246*(3–4), 288–304. https://doi.org/10.1016/j.epsl.2006.03.053

Kodaira, S., Iidaka, T., Kato, A., Park, J. O., Iwasaki, T., & Kaneda, Y. (2004). High pore fluid pressure may cause silent slip in the Nankai Trough. *Science*, *304*(5675), 1295–1298. https://doi.org/10.1126/science.1096535

Ladd, C. R., & Reber, J. E. (2020). The Effect of a Liquid Phase on Force Distribution During Deformation in a Granular System. *Journal of Geophysical Research: Solid Earth*, *125*(8), 1–17. https://doi.org/10.1029/2020JB019771

Leake, B. E., Woolley, A. R., Arps, C. E. S., Birch, W. D., Gilbert, M. C., Grice, J. D., et al. (1997). Nomenclature of amphiboles: Report of the subcommittee on amphiboles of the international mineralogical association, commission on new minerals and mineral names. *Canadian Mineralogist*, *35*(1), 219–246.

Lee, A. L., Stünitz, H., Soret, M., & Battisti, M. A. (2022). Dissolution precipitation creep as a process for the strain localisation in mafic rocks. *Journal of Structural Geology*, *155*(January), 104505. https://doi.org/10.1016/j.jsg.2021.104505

Leeman, J. R., Marone, C., & Saffer, D. M. (2018). Frictional Mechanics of Slow Earthquakes. *Journal of Geophysical Research: Solid Earth*, *123*(9), 7931–7949. https://doi.org/10.1029/2018JB015768

Misra, S., Boutareaud, S., & Burg, J. P. (2014). Rheology of talc sheared at high pressure and temperature: A case study for hot subduction zones. *Tectonophysics*, *610*, 51–62. https://doi.org/10.1016/j.tecto.2013.10.009

Moore, D. E., & Lockner, D. A. (2004). Crystallographic controls on the frictional behavior of dry and water-saturated sheet structure minerals. *Journal of Geophysical Research*, *109*(B3401), 1–16. https://doi.org/10.1029/2003jb002582

Moore, D. E., & Lockner, D. A. (2008). Talc friction in the temperature range 25°-400 °C: Relevance for Fault-Zone Weakening. *Tectonophysics*, *449*(1–4), 120–132. https://doi.org/10.1016/j.tecto.2007.11.039

Obara, K. (2002). Nonvolcanic deep tremor associated with subduction in southwest Japan. *Science*, *296*(5573), 1679–1681. https://doi.org/10.1126/science.1070378

Okamoto, A. S., Verberne, B. A., Niemeijer, A. R., Takahashi, M., Shimizu, I., Ueda, T., & Spiers, C. J. (2019). Frictional Properties of Simulated Chlorite Gouge at Hydrothermal Conditions: Implications for Subduction Megathrusts. *Journal of Geophysical Research: Solid Earth*, *124*(5), 4545–4565. https://doi.org/10.1029/2018JB017205

Penniston-Dorland, S. C., Gorman, J. K., Bebout, G. E., Piccoli, P. M., & Walker, R. J. (2014). Reaction rind formation in the Catalina Schist: Deciphering a history of mechanical mixing and metasomatic alteration. *Chemical Geology*, *384*, 47–61. https://doi.org/10.1016/j.chemgeo.2014.06.024

Penniston-Dorland, S. C., Kohn, M. J., & Piccoli, P. M. (2018). A mélange of subduction temperatures: Evidence from Zr-in-rutile thermometry for strengthening of the subduction interface. *Earth and Planetary Science Letters*, *482*, 525–535. https://doi.org/10.1016/j.epsl.2017.11.005

Phillips, N. J., Motohashi, G., Ujiie, K., & Rowe, C. D. (2020). Evidence of Localized Failure Along Altered Basaltic Blocks in Tectonic Mélange at the Updip Limit of the Seismogenic Zone: Implications for the Shallow Slow Earthquake Source. *Geochemistry, Geophysics, Geosystems*, *21*(7), 1–17. https://doi.org/10.1029/2019GC008839

Platt, J. P. (1975). Metamorphic and deformational processes in the Franciscan Complex, California: Some insights from the Catalina Schist terrane. *Bulletin of the Geological Society of America*, *86*(10), 1337–1347. https://doi.org/10.1130/0016-7606(1975)86<1337:MADPIT>2.0.CO;2

Platt, John Paul. (1976). *The petrology, structure, and geologic history of the Catalina Schist Terrain, Southern California*. University of California, Santa Barbara.

Raimbourg, H., Famin, V., Canizarès, A., & Le Trong, E. (2022). Fluid pressure changes recorded by trace elements in quartz. *Geochemistry, Geophysics, Geosystems*. https://doi.org/10.1029/2022GC010346

Rogers, G., & Dragert, H. (2003). Episodic tremor and slip on the Cascadia subduction zone: The chatter of silent slip. *Science*, *300*(5627), 1942–1943. https://doi.org/10.1126/science.1084783

Rooney, T. P., Riecker, R. E., & Gavasci, A. T. (1975). Hornblende deformation features. *Geology*, (July), 364–366.

Rutter, E. H., & Brodie, K. H. (2004). Experimental grain size-sensitive flow of hot-pressed Brazilian quartz aggregates. *Journal of Structural Geology*, *26*(11), 2011–2023. https://doi.org/10.1016/j.jsg.2004.04.006

Rybacki, E., & Dresen, G. (2004). Deformation mechanism maps for feldspar rocks. *Tectonophysics*, *382*(3–4), 173–187. https://doi.org/10.1016/j.tecto.2004.01.006

Sorensen, S. S. (1986). Petrologic and geochemical comparison of the blueschist and greenschist units of the Catalina schist terrane, southern California. *Blueschists and Eclogites*, 59–75.

Sorensen, S. S., & Barton, M. D. (1987). Metasomatism and partial melting in a subduction complex: Catalina Schist, southern California. *Geology*, *15*, 115–118.

Sorensen, S. S., & Grossman, J. N. (1989). Enrichment of trace elements in garnet amphibolites from a paleo-subduction zone: Catalina Schist, southern California. *Geochimica et Cosmochimica Acta*, *53*(1987), 3155–3177.

Soret, M., Agard, P., Ildefonse, B., Dubacq, B., Prigent, C., & Rosenberg, C. (2019). Deformation mechanisms in mafic amphibolites and granulites: Record from the Semail metamorphic sole during subduction infancy. *Solid Earth*, *10*(5), 1733–1755. https://doi.org/10.5194/se-10-1733-2019

Spandler, C., Hermann, J., Faure, K., Mavrogenes, J. A., & Arculus, R. J. (2008). The importance of talc and chlorite "hybrid" rocks for volatile recycling through subduction zones; evidence from the high-pressure subduction mélange of New Caledonia. *Contributions to Mineralogy and Petrology*, *155*(2), 181–198. https://doi.org/10.1007/s00410-007-0236-2

Wassmann, S., & Stöckhert, B. (2013). Rheology of the plate interface - Dissolution precipitation creep in high pressure metamorphic rocks. *Tectonophysics*, *608*, 1–29. https://doi.org/10.1016/j.tecto.2013.09.030

Webber, S., Ellis, S., & Fagereng, Å. (2018). "Virtual shear box" experiments of stress and slip cycling within a subduction interface mélange. *Earth and Planetary Science Letters*, *488*, 27–35. https://doi.org/10.1016/j.epsl.2018.01.035